Journal of Sustainable Development of Energy, Water and Environment Systems

http://www.sdewes.org/jsdewes

Year 2027, Volume 15, Issue 1, 1140759

Original Research Article

Effect of Operating Conditions on the Volumetric Mass Transfer Coefficient in a Laboratory-Scale Cooling Tower with Perforated Inclined Plates

Luis Guillermo Obregon Quiñones *, Samuel Andrés Sanchez Parra, Eladio Andrés Molina Lopez

Group on Sustainable Chemical and Biochemical Processes, Department of Chemical Engineering, Universidad del Atlántico, Carrera 30 # 8- 49, Puerto Colombia, Atlantico, Colombia

eladioamolina@mail.uniatlantico.edu.co (E.A.M.L.); sandressanchez@mail.uniatlantico.edu.co (S.A.S.P.)

*Correspondence: luisobregon@mail.uniatlantico.edu.co (L.G.O.Q.)

Cite as: Obregon-Quinones, L. G., Sanchez-Parra, S. A., Molina-Lopez, E. A., Effect of Operating Conditions on the Volumetric Mass Transfer Coefficient in a Laboratory-Scale Cooling Tower with Perforated Inclined Plates, J.sustain. dev. energy water environ. syst., 15(1), 1140759, 2027, DOI: https://doi.org/10.13044/j.sdewes.d14.0759

ABSTRACT

A laboratory–scale mechanical draft cooling tower equipped with eight sections of perforated inclined plates was designed to determine the effect of operating conditions on the volumetric mass transfer coefficient between water and air. A three–factor, three–level design of experiments was implemented, considering liquid mass flow rate (120, 240, and 360 kg/h), gas mass flow rate (36, 57, and 75 kg/h), and top water temperature (50, 60, and 70 °C). A total of 54 runs were performed, and the global volumetric mass transfer coefficient was calculated by combining energy and mass balances with the Mickley method. The experimental data were fitted to a power–law correlation using multivariable regression. The analysis of variance showed that top water temperature is the dominant factor, followed by liquid mass flow rate, whereas the influence of gas mass flow rate is comparatively small in the studied range. The selected correlation, based on the nominal gas flow rate, achieved a coefficient of determination of 0.869 and a root mean square error of 5.93×10^3 kg/(m^{3}h). The volumetric mass transfer coefficient values were found in the range from 4.6×10^3 to 6.2×10^4 kg/(m^{3}h). Vertical temperature profiles of water and air along the column revealed that, for high liquid flow rates, most of the cooling occurs in the lower stages, suggesting that the upper sections are underutilized.

KEYWORDS

Laboratory-scale cooling tower; evaporative cooling; volumetric mass transfer coefficient; operating conditions; perforated inclined plates.

INTRODUCTION

Cooling towers are one of the key components in industries, mainly used with the purpose of decreasing the temperature of hot liquids. In the case of the thermoelectric generation industry, the required cooling is responsible for approximately 10% of the total water demand in the world [1]. The thermal performance of the cooling towers is clearly explained in terms of varying air and water temperatures, as well as the driving potential for convection and evaporation heat transfer, along the height of the tower [2], In turn, operating conditions strongly influence tower performance and cooling effectiveness [3]. Furthermore, tower geometry and fill characteristics play a crucial role in determining the efficiency of the gas–liquid contact process [4]. Beyond thermal considerations, cooling water management and

* Corresponding author

environmental constraints associated with biofouling, plume formation, blowdown, and pressure drop continue to drive efforts toward improving tower efficiency [5].

Since the pioneering work of Merkel [6], numerous modelling approaches have been proposed to describe cooling tower performance. The effectiveness–NTU method was introduced as an alternative framework for cooling tower design and analysis [7]. Subsequent studies refined transfer characteristic correlations and improved the representation of fill performance under different operating conditions [8]. Other researchers revisited the classical Merkel formulation and proposed alternative procedures for cooling tower calculations [9]. More recently, numerical simulations and optimization-based methodologies have been employed to evaluate cooling tower behaviour under a wide range of environmental and operational conditions [10].

Alongside these modelling developments, experimental investigations have contributed significantly to the understanding of cooling tower operation. Studies conducted on pilot and industrial towers have examined the influence of liquid and gas flow rates on thermal performance [2], [3]. Numerical analyses of thermal-hydraulic behaviour have provided further insight into tower operation [11]. Experimental work has also demonstrated the influence of wet-bulb temperature variations in crossflow cooling towers [12], while transient operating conditions have been investigated through dynamic thermal analyses [13]. Additional studies evaluated the effects of flow parameters in mechanical-draft cooling towers [14]. The impact of fill configurations and operating strategies on tower efficiency has likewise been assessed experimentally [15].

Research efforts have also examined the role of packing design and internal tower configuration. Semi-empirical and optimization-based methods have been proposed to evaluate cooling tower performance under variable environmental conditions [10]. Experimental studies have assessed the performance of cooling towers equipped with different film packings [16]. The arrangement of cooling tower packing has also been shown to affect thermal performance and fluid distribution [17]. Similarly, seasonal climatic variations have been identified as an important factor influencing cooling tower efficiency [18]. Detailed analyses of liquid flow behaviour within cooling tower packing have provided further understanding of heat and mass transfer mechanisms [19]. Simulation-based studies have also been used to determine key operating parameters in mechanical-draft humidification towers [20].

Driven by the need to improve efficiency, reduce water consumption, and mitigate fouling, recent developments in cooling tower technology have focused on alternative fill materials and contact devices [4]. Different film fills, splash fills, and structured packings have been investigated to modify the hydrodynamics of the water film and enhance air–water interaction [17], [19]. Pressure-drop characteristics and energy consumption have also been evaluated as part of the design of alternative configurations [21]. Controlled laboratory towers are particularly valuable to test unconventional fills and to obtain high–quality data for correlation development. However, most works still focus on classical fills, while alternative geometries such as perforated inclined plates remain less explored.

The optimization of circulating cooling water systems has received increasing attention as industries seek to improve energy efficiency and support decarbonization efforts. Optimization strategies for cooling water networks have been proposed considering the influence of scaling and operational constraints [22]. The synthesis and optimal design of systems involving multiple cooling towers have also been investigated [23]. Other studies have focused on improving the operation of circulating water systems through variable-frequency drive implementation [24] and adaptive optimization algorithms [25]. Similar approaches have been applied to open circulating cooling water systems [26]. More recently, energy, exergy, and environmental criteria have been incorporated into cooling tower analysis to support sustainable operation [27]. In parallel, machine-learning and process-simulation techniques have expanded the capabilities of cooling water system optimization [28].

Reliable correlations for the volumetric mass transfer coefficient, $k_y a$, are fundamental for the successful implementation of these optimization frameworks. Accurate process models require representative mass-transfer correlations to predict cooling tower performance under different operating conditions [22]. The integration of process simulation tools with data-driven methodologies also depends on the availability of robust performance correlations [28]. Recent experimental and numerical studies have highlighted the importance of accurately characterizing heat and mass transfer processes when evaluating cooling towers equipped with alternative packing configurations [29]. Likewise, performance enhancement strategies based on modified packing designs and nanofluids have demonstrated the strong influence of mass-transfer characteristics on overall tower efficiency [30]. Consequently, correlations for $k_y a$ should capture not only the influence of tower geometry but also the sensitivity of mass transfer to changes in operating conditions.

The primary novelty of this work lies in the generation of a comprehensive experimental dataset and the development of a specific empirical correlation for a laboratory-scale counterflow cooling tower equipped with perforated inclined plates. Unlike conventional film fills that rely on continuous surface wetting, or splash fills that depend on droplet generation, perforated inclined plates offer a unique hydrodynamic behaviour by combining film flow along the incline with droplet fall through the perforations. This less-documented contact geometry presents an alternative for enhancing gas-liquid interaction.

MATHERIAL AND METHODS

This section plans the methodological framework, experimental setup, and analytical procedures used to evaluate the performance of the laboratory-scale cooling tower. It details the physical characteristics of the experimental facility, the instrumentation employed for data collection, the mathematical modelling based on the Mickley method, and the statistical design of experiments applied to analyse the operating variables.

Experimental facility

Experiments were run in a counterflow mechanical–draft cooling tower located at the Heat and Mass Transfer Laboratory of Universidad del Atlántico, see figure 1. The column was built in transparent acrylic, Figure 2, which allows visual inspection of the flow, and was divided into seven identical stages, which had seven perforated inclined plates. Each plate was mounted at a fixed angle with respect to the horizontal and perforated with uniformly distributed circular holes to enhance the air– water contact. The design and hydrodynamic characterization of similar units have been reported in previous works [29], [31], [32].

Warm water from a storage tank (see figure 1) was pumped by a multistage centrifugal pump (P–101) to the top of the column, where it was distributed through the top plate. Water flows down by gravity through all the stages and is collected at the bottom in a container. Ambient air was supplied by a centrifugal blower (K–101) and introduced at the base of the column, where it flowed upward in counter-current to the water stream. The air flow rate was changed by a variable–frequency drive (VFD–101) installed on the blower.

Water temperatures were measured at the inlet and outlet of the column and at intermediate heights using calibrated Pt100 resistance thermometers with an uncertainty of ±0.1 °C. Air dry–bulb temperature and relative humidity at the inlet and out-let are measured with similar Pt100 sensors. All the measures were used to determine the air enthalpy and humidity ratio via psychrometric relationships [33], [34]. Liquid and gas flow rates were determined by a flowmeter and an anemometer, respectively. All signals were reported through a data acquisition system and recorded once the steady state was reached.

A simplified process flow diagram is shown in Figure 1, and a photograph of the experimental setup is presented in Figure 2.

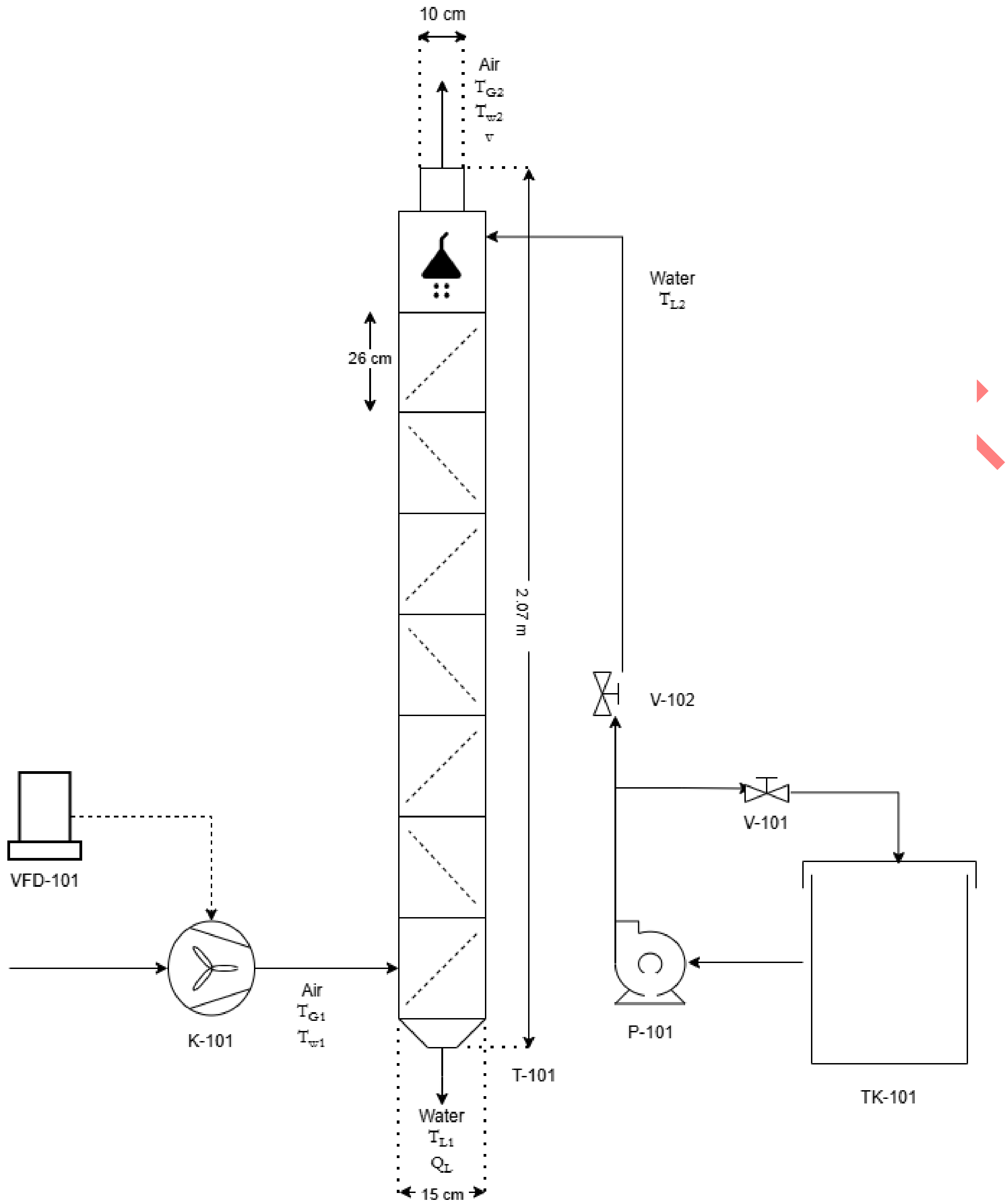

Figure 1. Process flow diagram of the laboratory cooling tower. T–101: cooling tower with perforated inclined plates; TK–101: water storage tank; P–101: multistage pump; K–101: centrifugal blower; V–101 and V–102: manual valves; VFD–101: variable–frequency drive.

Figure 2. Laboratory cooling tower system with perforated inclined plates and associated equipment.

Figure 3 shows the fill used in the cooling tower. This fill consists of an acrylic plate inclined at an angle of 60° with respect to the horizontal. The plate contains 350 perforations distributed in a matrix arrangement, which allows the water to pass through the plate and increases the contact area between water and air. The main dimensions of the inclined plate and the arrangement of the orifices are presented in Figure 3. The plate thickness is 4 mm, hole diameter is 3 mm, contact area of the plate is 906.21 cm^2, porosity of the plate is 0.0621, stage spacing 25 mm, and the cross section is 15 cm x 15 cm.

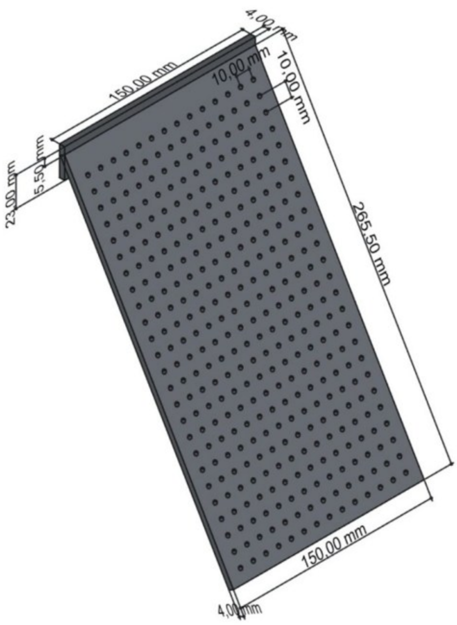

Figure 3. Fill of the cooling tower: dimensions of the inclined plate with multiple orifices.

Figure 4 illustrates the main phenomena occurring on the inclined plate during the operation of the cooling tower. The blue arrows represent the flow of hot water, while the red arrows represent the upward flow of air. The hot water enters the tower from the upper section with the help of a pump and is distributed over the fill by sprinklers. Once the water reaches the inclined plate, it flows downward along the surface due to gravity.

As the water moves over the plate, part of it passes through the orifices and falls onto the next plate located below. The seven plates were arranged alternately, so the direction of water flow changes from one plate to the next. This arrangement increases the residence time of the water inside the tower and improves the interaction between the liquid and gas phases.

At the same time, air is introduced from the bottom of the tower by a blower and moves upward, opposite to the general direction of the water flow. This counter-current contact allows heat to be transferred from the hot water to the air. In addition, part of the water evaporates, producing mass transfer and contributing to the cooling process.

The presence of multiple orifices in the inclined plate improves the distribution of the water and promotes greater contact between water and air. Therefore, the perforated inclined plates help enhance heat and mass transfer, increasing the overall efficiency of the cooling tower.

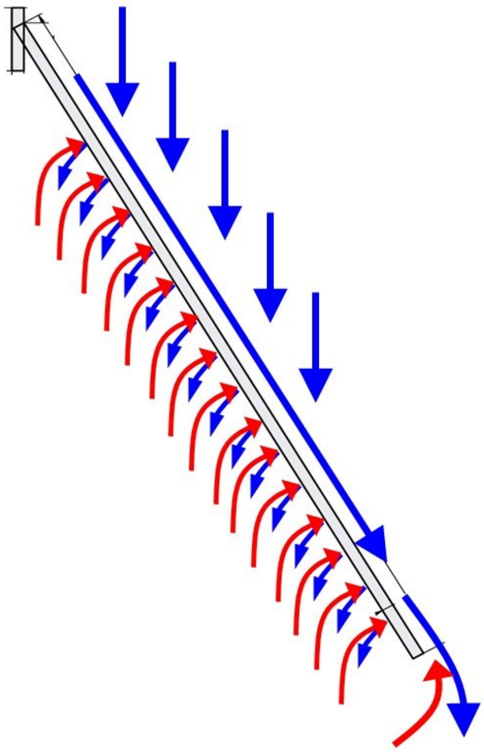

Figure 4. Water–air contact on the inclined plate with multiple orifices.

This fill, Figure 4, can be placed as a hybrid-type experimental fill because it is not a conventional film, not a pure splash fill, and not a typical grid fill. This is the novelty of this work. It combines water-film flow over inclined surfaces with droplet formation through multiple orifices, which increases the air-water contact and the residence time. This film works as a film fill because it allows water to flow over a solid surface. It works like a splash because the holes interrupt the film and redistribute water and generates droplets between plates increasing the air-water contact. Another comparison is with grid fills which has lower heat transfer performance than film fill, but it is more resistant to blockage. The inclined holed plates may share part of this advantage because the orifices and open spaces can reduce the risk of forming a continuous clogged channel. The experimental dataset and the empirical correlation developed in this study provide specific information for a hybrid perforated inclined plate fill configuration.

Design of experiments

The effect of the operating conditions on the global volumetric mass transfer coefficient $k_y a$ was studied considering a three–factor, three–level, two-replicate design of experiments resulting in 27 distinct combinations and a total of 54 experiments. The selected factors, shown in Table 1, were liquid mass flow rate L; gas mass flow rate G; and top water temperature T_{L2}. The levels were chosen based on preliminary tests and on the hydraulic and thermal limitations of the experimental setup, following standard DOE principles [35], [36].

Table 1. Factors and levels used in the design of experiments.

Factor	Symbol	Level 1 (Low)	Level 2 (Medium)	Level 3 (High)
Liquid mass flow rate (kg/h)	L	120	240	360
Gas mass flow rate (kg/h)	G	36	57	75
Top water temperature (◦C)	T_{L2}	50	60	70

The system reached steady state for each experiment (based on stable temperatures and flow rates). Figure 5 illustrates the experimental domain in the L–G–T_{L2} space. The selected levels ensure that flooding or severe entrainment did not occur.

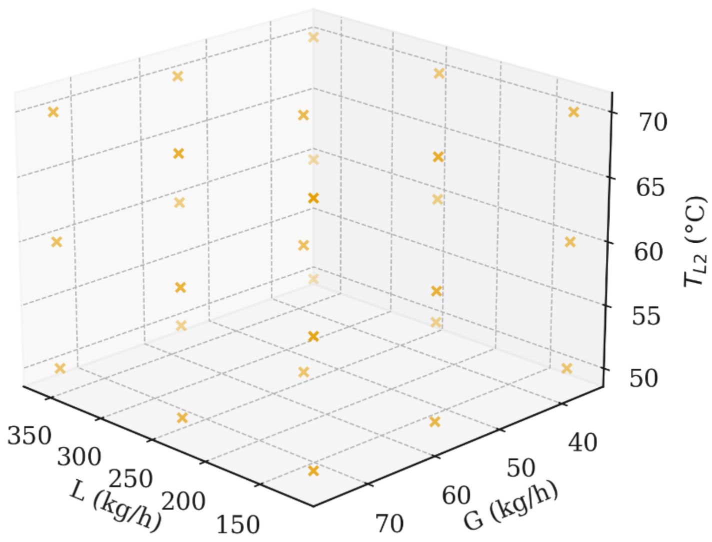

Figure 5. Schematic representation of the 3-factorial design of experiment in the space of liquid mass flow rate L, gas mass flow rate G, and top water temperature T_{L2}.

Thermodynamic framework and calculation of the volumetric mass transfer coefficient

The analysis of mass and heat transfer is based on Merkel's classical approach [6], [37]. For a differential height dZ in a counterflow cooling tower, the energy balance in the gas phase is expressed as:

$$G'_s\, dh_y = k_y a \left(h_{yi} - h_y\right) dZ = h_L a (T_L - T_i) dZ \tag{1}$$

where G_s' is the dry-air mass flux, h_y is the bulk air enthalpy, and h_{yi} is the air enthalpy at the interface, evaluated at saturation conditions corresponding to the interface temperature T_i [38], [39]. Integrating equation (1) over the total column height (Z) yields the overall volumetric mass transfer coefficient ($k_y a$):

$$k_y a = \frac{G_s'}{Z} \int_{h_{y,1}}^{h_{y,2}} \frac{d h_y}{h_{yi} - h_y} \tag{2}$$

The integration limits $h_{y,1}$ and $h_{y,2}$ represent the air enthalpies at the inlet (bottom) and outlet (top) of the tower, respectively, which are determined from the experimental psychrometric data. To solve the integral in equation (2), it is essential to establish the profile of h_{yi} corresponding to each h_y value along the column. Theoretically, the bulk fluid conditions on the operating line (T_L, h_y) are linked to the interface conditions on the equilibrium line (T_i, h_{yi}) via a tie line, whose slope is defined by the ratio of the individual heat and mass transfer coefficients:

$$\frac{h_y - h_{yi}}{T_L - T_i} = -\frac{h_L a}{k_y a} \tag{3}$$

Since the slope of the tie line $\left(-\frac{h_L a}{k_y a}\right)$ is unknown a priori and varies for each experiment, a global degree of freedom is introduced. To close the system of equations and simultaneously determine the gas temperature profile (T_G), Mickley's geometric method was implemented [33]. Accordingly, the operating line was discretized into multiple equivalent water temperature intervals between the bottom (subscript 1) and the top (subscript 2) of the tower.

This allows the air enthalpy at the beginning ($h_{y,n}$) and end ($h_{y,n+1}$) of each interval to be known in advance via localized mass and energy balances.

To ensure the strict reproducibility of this research, the calculation procedure was structured using the following dual-iteration algorithm, mathematically resolved via the Solver tool to handle the complex system of coupled equations:

- **Definition of boundary conditions**: The experimental extreme process measurements are introduced: at the bottom ($T_{L,1}$, $h_{y,2}$ and the measured outlet gas temperatura $T_{G,2,exp}$).
- **Outer Loop (Global convergence)**: An initial unique value is assumed for the global slope of the tie line $-\frac{h_L a}{k_y a}$.
- **Inner Loop (Sequential Geometric Calculation):** The inner loop consists in the determination of the interface point, estimation of the new gas temperature and finally de interval advancement:
  - **Determination of the interface point:** Using the known $T_{L,n}$ and $h_{y,n}$ values at the start of the Interval, the slope $-\frac{h_L a}{k_y a}$ is applied in equation (3) to project the tie line until its intersection with the water saturation curve, thereby obtaining the local interface conditions ($T_{i,n}$ and $h_{yi,n}$).
  - **Estimation of the new gas temperature**: According to Mickley's geometric formulation, a gas-phase transfer line is drawn connecting the bulk air conditions ($T_{G,n}$, $h_{y,n}$) with the interface point ($T_{i,n}$, $h_{yi,n}$) of that specific interval. The equation of this line is expressed as:

$$\frac{h - h_{\mathrm{y,n}}}{T - T_{\mathrm{G,n}}} = \frac{h_{\mathrm{yi,n}} - h_{\mathrm{y,n}}}{T_{\mathrm{i,n}} - T_{\mathrm{G,n}}} \tag{4}$$

Since the air enthalpy at the end of the interval ($h_{\mathrm{y,n+1}}$) is known from the operating line, a horizontal projection is drawn to evaluate the line described in equation (4). Solving analytically yields the exact gas temperature for the next interval ($T_{\mathrm{G,n+1}}$):

$$T_{\mathrm{G,n+1}} = T_{\mathrm{G,n}} + \left(h_{\mathrm{y,n+1}} - h_{\mathrm{y,n}}\right)\left[\frac{T_{\mathrm{i,n}} - T_{\mathrm{G,n}}}{h_{\mathrm{yi,n}} - h_{\mathrm{y,n}}}\right] \tag{5}$$

- **Interval advancement**: The algorithm takes the computed ($h_{\mathrm{y,n+1}}$, $T_{\mathrm{G,n+1}}$) values as the new initial conditions for step n+1 and repeats the process sequentially until all the intervals are completed, reaching the top of the column. The iteration ends when the temperature of the gas in the last interval is equal to the temperature of the gas at the top of the column.

Once system convergence is achieved, the mathematical algorithm simultaneously provides the true slope $-\frac{h_{\mathrm{L}}a}{k_{\mathrm{y}}a}$ for the run, the gas temperature profile, and a set of n (number of intervals) coupled enthalpy data points (h_{y}, h_{yi}) along the entire column.

Mathematical analysis of this coupled data profile (h_{y}, h_{yi}) demonstrated a remarkably robust linear relationship. To prevent numerical truncation errors associated with traditional integration methods (such as Simpson's or trapezoidal rules) and to enhance the exact reproducibility of the model, the following empirical relationship was formulated:

$$h_{\mathrm{yi}} = Ah_{\mathrm{y}} + B \tag{6}$$

It must be emphasized that the coefficients A and B are not global constants but are run-specific fitting parameters, calculated via linear regression of the n-point profile generated exclusively for that individual run in the preceding step.

Finally, substituting the linear relationship (equation 6) into Merkel's integral (equation 2) yields an exact analytical solution:

$$k_{\mathrm{y}}a = \frac{G'_{\mathrm{s}}}{Z}\int_{h_{\mathrm{y,1}}}^{h_{\mathrm{y,2}}} \frac{dh_{\mathrm{y}}}{\left(Ah_{\mathrm{y}} + B\right) - h_{\mathrm{y}}} = k_{\mathrm{y}}a = \frac{G'_{\mathrm{s}}}{(A-1)Z}\int_{h_{\mathrm{y,1}}}^{h_{\mathrm{y,2}}} \frac{dh_{\mathrm{y}}}{h_{\mathrm{y}} - \dfrac{B}{A-1}} \tag{7}$$

Direct resolution of equation (8) leads to the final explicit expression used in this study to determine the overall volumetric mass transfer coefficient:

$$k_{\mathrm{y}}a = \frac{G'_{\mathrm{s}}}{(A-1)Z}\ln\left[\frac{h_{\mathrm{y,2}}(A-1) + B}{h_{\mathrm{y,1}}(A-1) + B}\right] \tag{8}$$

This hybrid approach leverages the capability of solver and Mickley's method to map the internal column conditions, but utilizes a final analytical integration guided by the constants A and B, effectively eliminating any numerical uncertainty in the calculation of $k_{\mathrm{y}}a$.

Temperature profiles along the column

Since the Mickley method links the enthalpy of moist air to its temperature, the air temperature variation along the column was plotted as a function of height. A similar procedure was applied to determine the water temperature profile, allowing a direct comparison of the thermal behaviour of both streams along the column [33], [34].

Temperature profiles were obtained for gas flow rate $G = 36$, 57, and 75 kg/h and top water temperature $T_{L2} = 50$, 60, and 70°C, keeping the liquid mass flow rate within the range $L = 120–360$ kg/h.

Psychrometric representation and temperature-enthalpy profiles

In addition to the vertical temperature profiles, the evolution of the air-water contact along the column was analyzed on a psychrometric temperature-enthalpy diagram. The specific enthalpy of humid air, h_y, was calculated from the line of operation.

For selected operating conditions, the air states at the inlet and outlet of each stage were represented on a T-h_y diagram along with the wet air saturation curve. This diagram is obtained directly from the Mickley method and allows the humidification process of the column along its length to be perfectly observed.

In this work, detailed T-h_y profiles are presented for a fixed gas mass flow rate, G=36 kg/h, and three values of the top water temperature $T_{L2} = 50$, 60, and 70 °C. For each T_{L2}, the three liquid mass flow rates L=120, 240, and 360 kg/h were considered. These profiles are used to interpret the increase in moisture content of the air and its proximity to saturation under different operating conditions.

Statistical analysis and model fitting

The experimental design and statistical analysis were carried out using analysis of variance (ANOVA) [35], [36]. The following power–law correlation was proposed:

$$k_y a = K\, T_{L2}^{\alpha} G^{\beta} L^{\gamma} \tag{9}$$

which becomes linear in logarithmic form:

$$\ln(k_y a) = \ln K + \alpha \ln T_{L2} + \beta \ln G + \gamma \ln L \tag{10}$$

Parameters K, α, β, and γ were estimated via multiple linear regression on equation (10). The model was created with 75% of the experiments. The remaining samples were used as prediction data for the model, and thus, observe the behaviour of statistical metrics such as the root mean square error of prediction (RMSE), see equation (11), and R^2 using the total data to know the reliability of the model.

$$\text{RMSEP} = \sqrt{\frac{1}{n}\sum_{i=1}^{n}\left(k_y a_{\text{exp},i} - k_y a_{\text{pred},i}\right)^2} \tag{11}$$

Where n is the number of observations. The ANOVA was used to evaluate the significance of each factor and to verify the adequacy of the model at a significance level α-*value* = 0.05.

Estimation and prediction of outlet water temperature

To provide practical applicability to the developed mass transfer model, an additional analysis was carried out to estimate and predict the outlet water temperature (T_{L1}) of the cooling tower. The prediction of T_{L1} is a key operational variable in cooling tower design and performance evaluation, as it directly reflects the thermal effective-ness of the gas–liquid contact and the influence of operating conditions.

The estimation of T_{L1} was performed using the previously obtained volumetric mass transfer coefficient ($k_y a$) correlation, combined with the energy and mass balance formulation applied along the height of the column. For a given set of operating conditions (liquid mass flow rate L, gas mass flow rate G, and inlet water temperature at the top of the column T_{L2}), the model allows to predict the outlet water temperature.

Experimental measurements of T_{L1} were obtained for each operating condition and compared with the corresponding model predictions. To quantitatively evaluate the predictive capability of the model, the root mean square error of prediction (RMSEP) was calculated, as well as the root mean square error of cross-validation (RMSECV).

RESULTS AND DISCUSSION

The experimental results are presented and discussed to evaluate how the operating conditions affect the cooling process performance. The analysis begins with the individual effects of fluid flow rates and inlet water temperature on the volumetric mass transfer coefficient, followed by a detailed evaluation of the mass transfer coefficients, and concludes with the validation of the predictive mathematical and statistical models.

Behaviour of operating conditions on the volumetric mass transfer coefficient

To analyze the behavior of the volumetric mass transfer coefficient (k_ya) more closely, it was plotted as a function of T_{L2} for different combinations of L and G (see Figures 4 and 5). In Figures 6(a), (b), and (c), the values of k_ya are presented for different air mass flow rates (36, 57, and 75 kg/h) while keeping the water flow rate fixed in each case. For a given water inlet temperature (T_{L2}), the curves show very similar k_ya values, indicating that increasing the air flow does not produce significant variations in the mass transfer coefficient within the experimental range. This confirms that the influence of air flow is low compared to the other operating variables, which is consistent with the statistical analysis, where the air flow was the least significant variable.

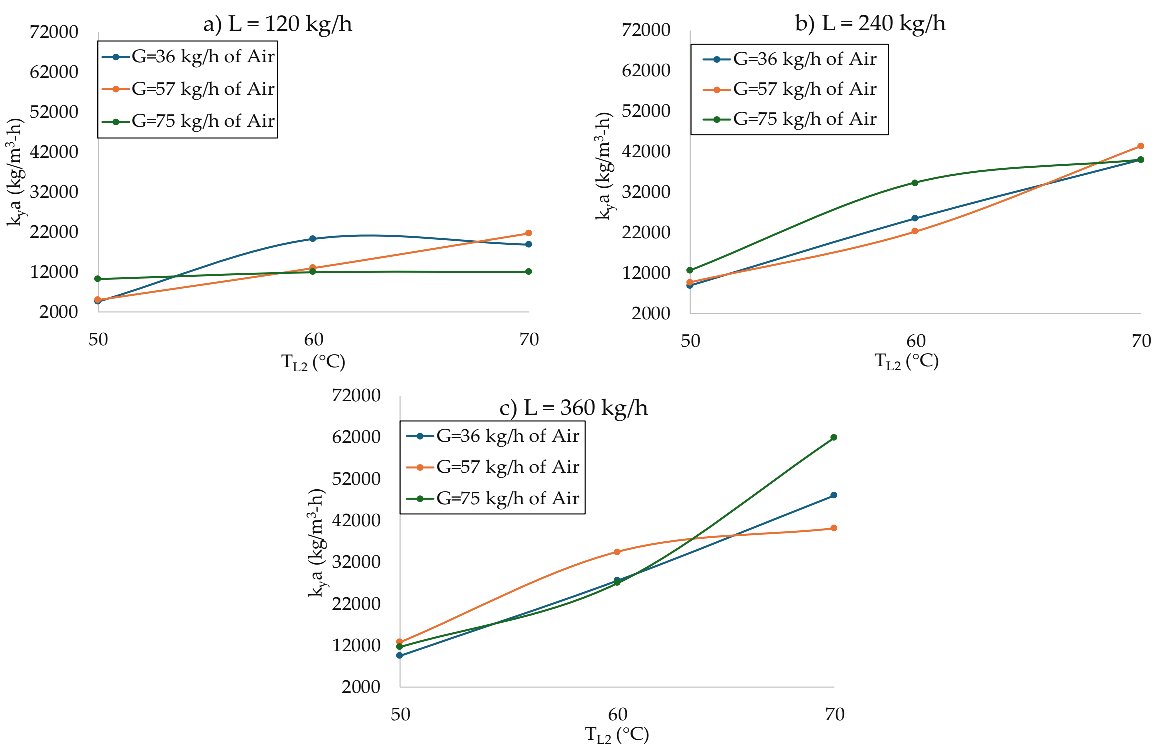

Figure 6. Experimental volumetric mass transfer coefficient k_ya as a function of top water temperature T_{L2} for different gas flow rates at (a) L = 120 kg/h, (b) L = 240 kg/h, and (c) L = 360 kg/h.

In Figure 7, the behavior of $k_y a$ is shown for different water flow rates (120, 240, and 360 kg/h) while keeping the air flow constant. It was found that $k_y a$ always increases with the liquid flow rate for the same T_{L2}, indicating a positive effect of the water flow on mass transfer. As the water inlet temperature increases, particularly above 60 °C, the curves begin to diverge, and the differences in $k_y a$ values become more pronounced, reflecting a nonlinear response of the system under conditions of higher thermal energy. At high inlet water temperatures, small variations in the liquid flow produce amplified changes in $k_y a$ and, therefore, in evaporation. Overall, the results in Figure 7 confirm that T_{L2} is the variable with the greatest impact, followed by the water flow rate, while the effect of the air flow is minimal within the studied range. Besides, it can be seen in Figure 8 that the behavior of the $k_y a$ is almost linear with T_{L2} when G is changed for the different values of L. However, this pattern changes to a nonlinear trend when G is constant.

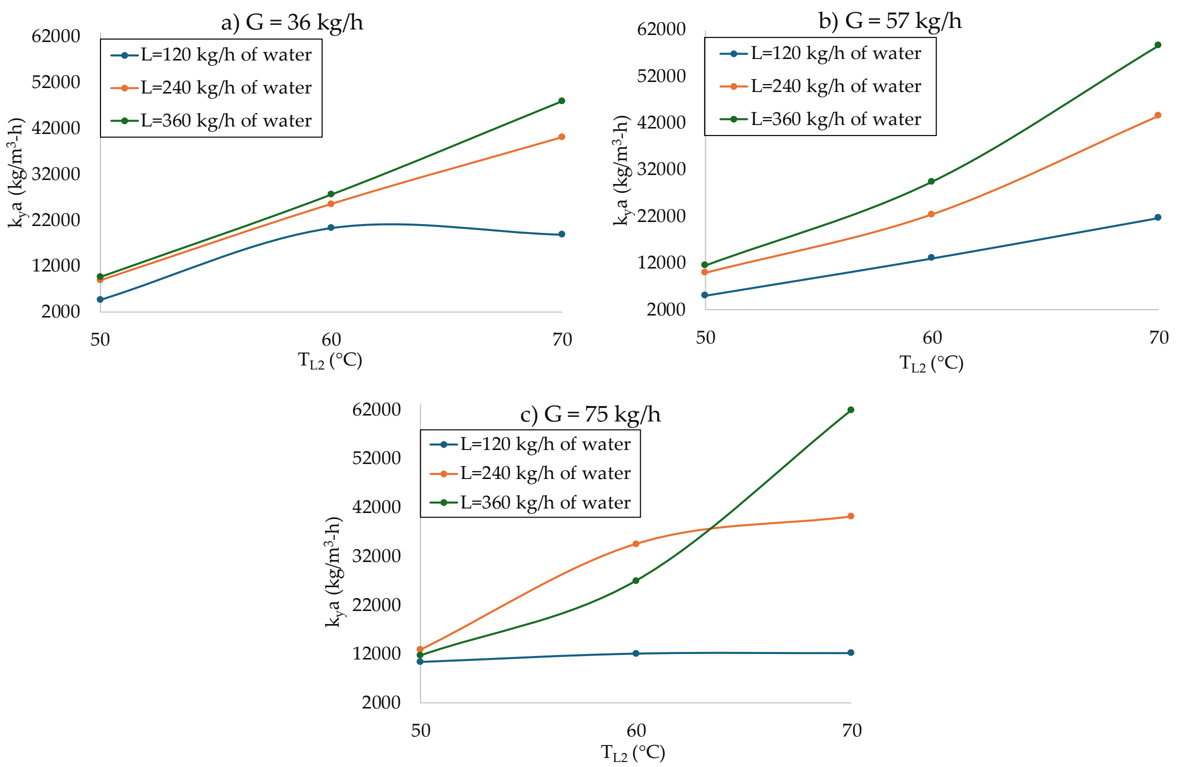

Figure 7. Experimental volumetric mass transfer coefficient $k_y a$ as a function of top water temperature T_{L2} for different liquid flow rates.

Temperature profiles along the column

Figure 8–10 shows the temperature profiles of water and air along the column height for different gas flow rates. For each G, three subplots are presented corresponding to top water temperatures T_{L2} = 50, 60, and 70 ◦C, and each subplot includes the three liquid mass flow rates (L = 120, 240, and 360 kg/h).

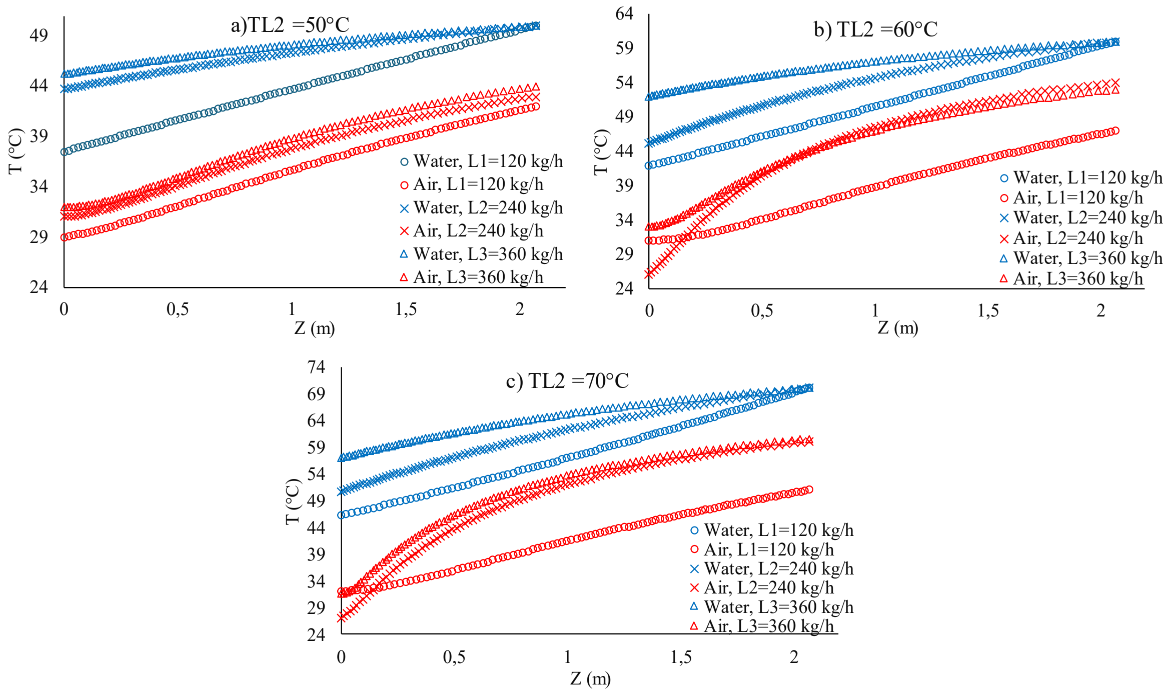

Figure 8. Vertical temperature profiles of water and air along the column for G = 36 kg/h, liquid mass flow rates (L = 120, 240, and 360 kg/h), and temperatures (T_{L2}= 50, 60, and 70 °C).

For G = 36 kg/h (Figure 8), the water temperature generally decreases almost linearly from the inlet to the outlet at L = 120 kg/h, while the air temperature increases almost linearly as well, indicating a uniform thermal driving force along the height of the tower. As L increases to 240 and 360 kg/h, a higher amount of water temperature drop occurs in the lower part of the column, whereas the upper stages exhibit smaller gradients.
A similar behavior is observed for G = 57 and 75 kg/h (Figures 9 and 10). Increasing T_{L2} amplifies the temperature difference at the bottom of the column, resulting in steeper gradients in the first stages, specifically at the highest liquid flow rate. In all cases, the air temperature rises clearly in the lower sections, and then it tends to have a small variation towards the top, resulting in a rapid uptake of heat and moisture near the water outlet.
At high L and high T_{L2}, most of the cooling is concentrated in the lower part of the column, so the extra packing height in the upper stages is not totally exploited.

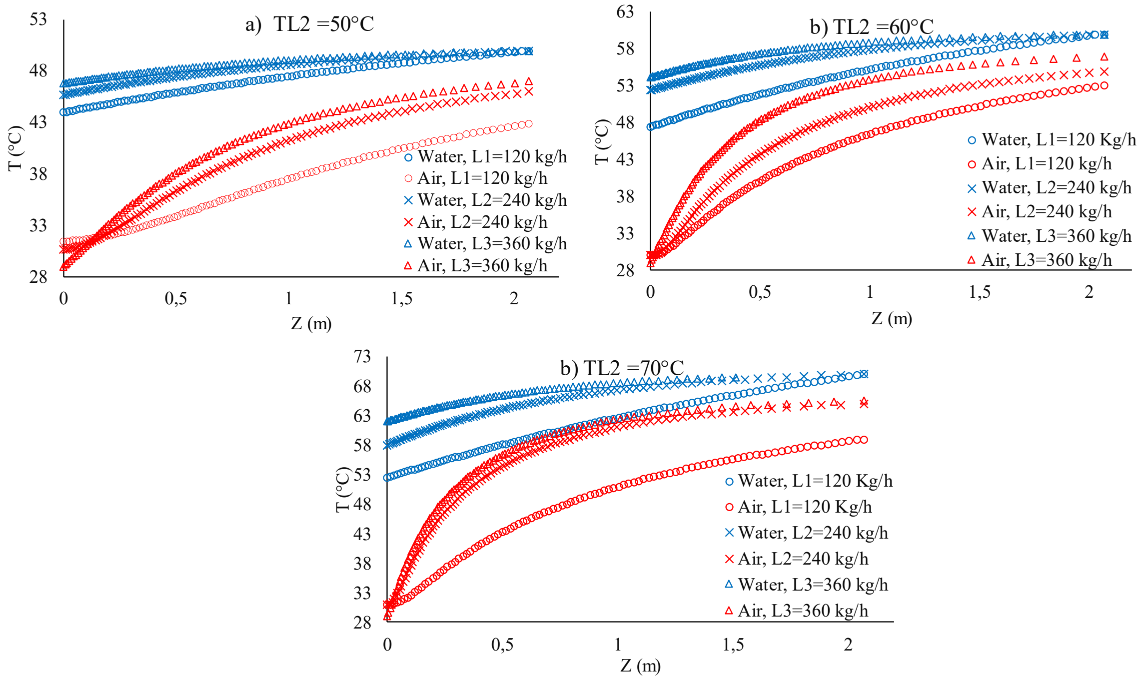

Figure 9. Vertical temperature profiles of water and air along the column for G = 57 kg/h, liquid mass flow rates (L = 120, 240, and 360 kg/h), and temperatures (T_{L2}= 50, 60, and 70 °C).

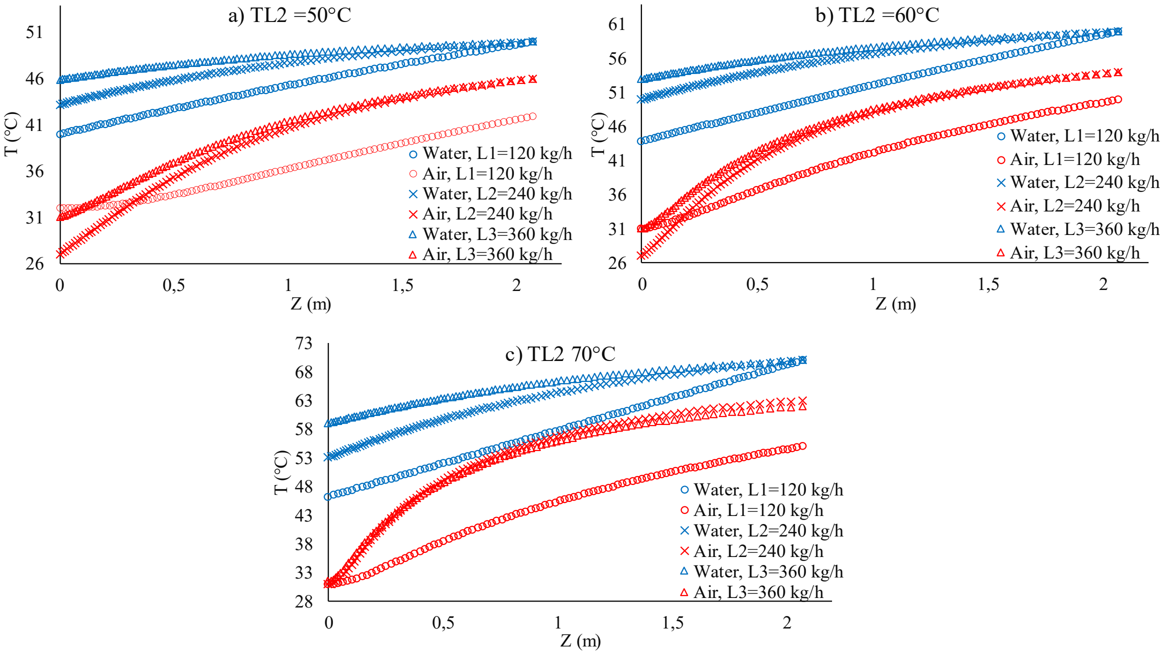

Figure 10. Vertical temperature profiles of water and air along the column for G = 75 kg/h, liquid mass flow rates (L = 120, 240, and 360 kg/h), and temperatures (T_{L2}= 50, 60, and 70 °C).

Psychrometric temperature-enthalpy profiles

Figure 11 shows the enthalpy of the gas as a function of the gas temperature (curved lines) and the water temperature (straight lines) for G=36 kg/h at three inlet water temperatures, T_{L2}= 50, 60, and 70 °C. Each group corresponds to three liquid mass flow rates L=120, 240, and 360 kg/h, plotted together with the equilibrium or saturation line of air (dashed curve). The lowest part of the lines corresponds to the bottom of the column, and the upper part of the lines corresponds to the top.

For T_{L2} = 50 °C, the operating lines (straight lines) on the T–h_y diagram remain relatively far from the saturation line, indicating that the system maintains a strong driving force for both heat and mass transfer. In general, a larger separation between the operating and saturation lines corresponds to more effective heat and mass transfer.

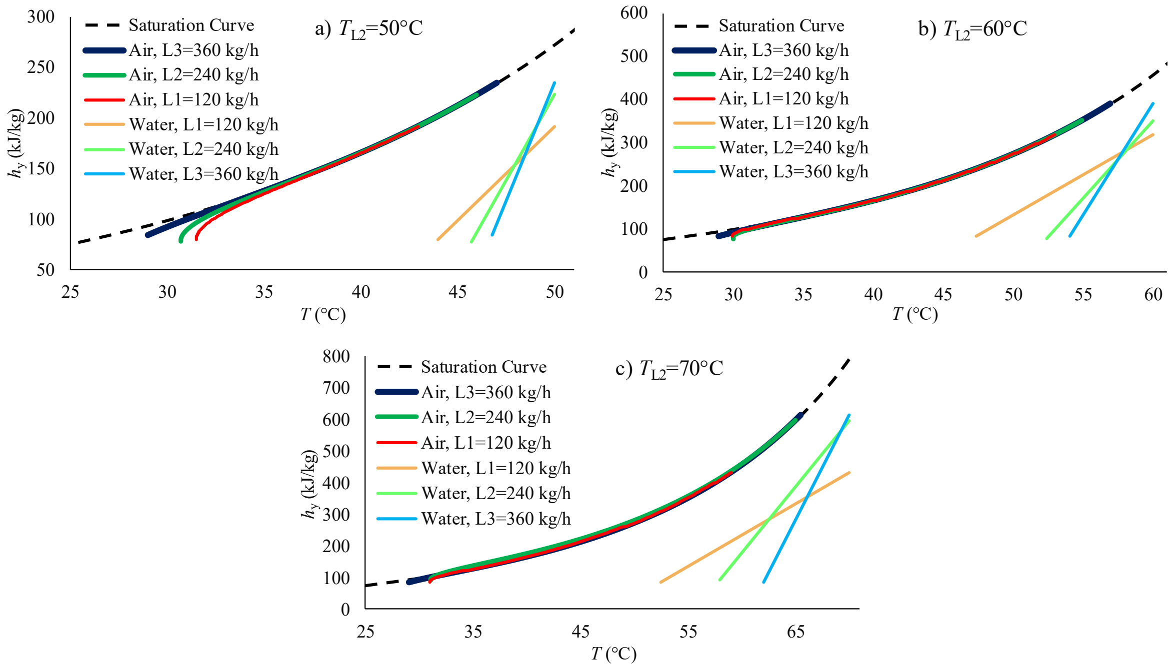

Figure 11. Gas enthalpy profile as a function of the gas temperature (curved lines) and the water temperature (straight lines) for G=36 kg/h.

For all cases shown, the separation between the operating and equilibrium lines is greater at the bottom of the tower than at the top. This indicates that heat transfer is more intense in the lower section of the tower. Additionally, for all the plots, the air at the bottom is not fully saturated, which enhances heat transfer due to increased water evaporation. Consequently, the bottom of the tower is more efficient than the upper section, as a larger fraction of the total heat transfer occurs in this region. The mentioned effect is more pronounced for liquid mass flow rate L=240 and 360 kg/h, because the slope of both straight lines increases causing more heat transfer in the bottom than in the top. Also, in all cases the air temperature profiles are very close to each other until overlapping reaching the saturation line, indicating that the air rapidly reaches conditions of 100% relative humidity inside the tower. This suggests that the air saturation occurs near in a place near the bottom of the column and is maintained along the rest of the height. Therefore, the heat transfer in the upper section is dominated by sensible heating of saturated air, while the latent contribution is comparatively more important near the bottom.

Regression models and analysis of variance for the volumetric mass transfer coefficient

Table 2 summarizes the parameters obtained for the proposed power-law correlation shown in equation (9). The exponents indicate that $k_y a$ increases strongly with T_{L2} and more moderately with the liquid mass flow rate L, while the effect of the gas mass flow rate G is relatively small.

Table 2. Regression coefficients for the power-law correlation of the volumetric mass transfer coefficient.

Model	K	α	β	γ

Proposed model (nominal *G*)	$6.59x10^{-6}$	4.173	0.149	0.756

The corresponding regression statistics are presented in Table 3. The model yields R^2 = 0.869 and RMSE = 5.93 × 10^3 kg/(m^3·h), which are acceptable values for representing the trends found with the experimental data. The empirical correlation obtained can be written as follows in Equation (12).

$$k_y a = 6.59 \times 10^{-6} T_{L2}{}^{4.173} G^{0.149} L^{0.756} \tag{12}$$

This equation lies within the range of exponents reported in the literature for cooling towers with different fills and geometries [3], [16], [32]. The correlation is specific to the tower investigated. Its explicit dependence on T_{L2}, G, and L makes it suitable for integration into models of circulating cooling water systems and for preliminary design calculations.

Table 3. Regression statistics for the proposed power-law correlation.

Model	R^2	RMSE [kg/(m^3·h)]	Number of experiments
Proposed model (nominal *G*)	0.869	5.93 × 10^3	54

An analysis of variance (ANOVA) for the fitted regression model is presented in Table 4, and according to the *p-values*, the hot water inlet temperature, (T_{L2}), and the liquid mass flow rate, (L), had a statistically significant effect on $k_y a$ within the evaluated operating range, with *p-values* lower than 0.05. In contrast, the air mass flow rate, (G), did not show a statistically significant effect as indicated by its *p-value* of 0.518.

Table 4. Analysis of variance (ANOVA) for the volumetric mass transfer coefficient $k_y a$.

Source	***DF***	***SS***	***MS***	***F***	***P-value***
T_{L2}	2	7175087629	3587543 815	52.11	0.000
G	2	91834930	45917465	0.67	0.518
L	2	3613427758	1806713879	26.24	0.000
Error	47	3235 831068	68847470	–	–
Total	53	14116181386	–	–	–

The results presented in Table 4 are also shown in the main effects plot shown in Figure 12. $k_y a$ values increased significantly with T_{L2}, which may be attributed to higher driving force for heat and mass transfer at higher temperatures. Also, increasing L results in higher $k_y a$ values, probably due to improved wetting and water distribution over the inclined perforated plates. Although G showed a slight increasing trend in $k_y a$, its effect was not statistically significant within the evaluated range. The influence of G should be interpreted with caution. It doesn't imply that the air mass flow rate has no effect on the cooling tower performance in general. Its effect was not significant only for the specific experimental conditions and geometry evaluated in this study. Extrapolation outside the tested range is not recommended.

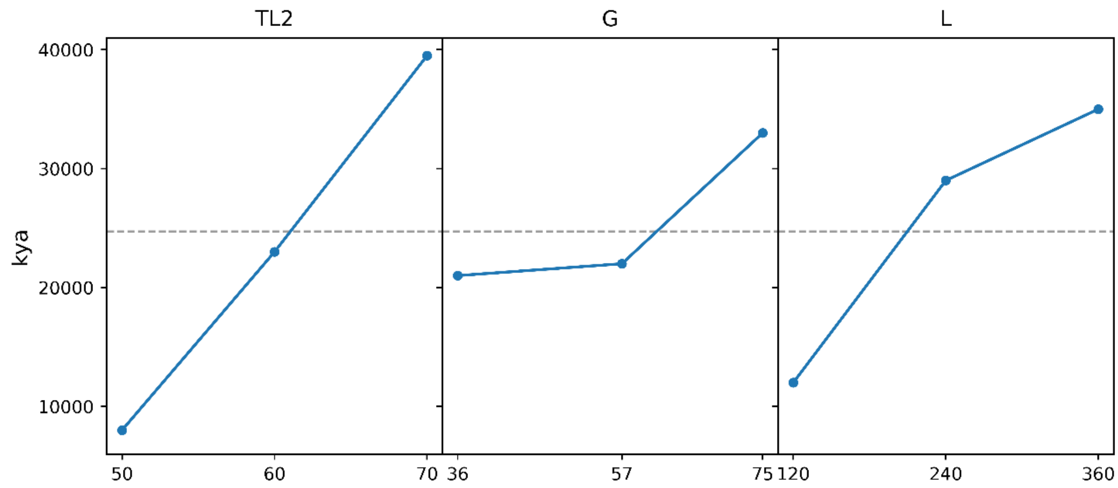

Figure 12. Main effects plot for the volumetric mass transfer coefficient k_ya

Figure 13 presents the interaction plots obtained from the fitted model. In the range studied, any of the parameters have significant effects on the k_ya values. In the next subdivision, a more detailed analysis will be presented for all the parameters.

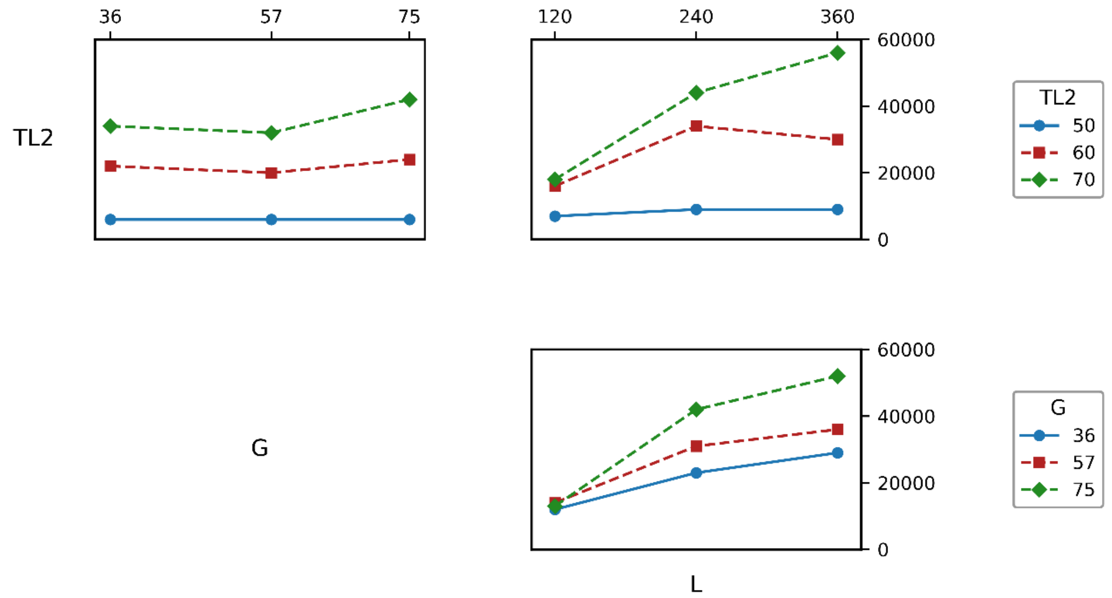

Figure 13. Three-factor Interaction plot for the volumetric mass transfer coefficient k_ya

Estimation and prediction of the outlet water temperature

The predictive capability of the developed model was evaluated through the estimation of the outlet-water temperature (T_{L1}), which is a key operational variable directly related to the thermal performance of the cooling tower. Outlet-water temperature predictions were compared against experimental measurements using the RMSEP (Root Mean Square Error of Prediction) and RMSECV (Root Mean Square Error of Cross-Validation) to assess the predictive model accuracy. Their values are reported in Table 5.

Table 5. Regression statistics for the Outlet Water Temperature estimation.

Key metric	Error

RMSEP	10.70
RMSECV	4.54

These results indicate low errors for both prediction and cross-validation. It means that the model can be used to estimate the outlet water temperature at different operating conditions.

Figure 14 presents the comparison between measured and predicted values of T_{L1} for the prediction dataset. In general, the model describes the overall trend of the experimental data, with most predicted temperatures following the same increasing pattern observed in the measurements. However, noticeable deviations are observed for a limited number of experiments, where the predicted temperatures significantly underestimate the measured values. These discrepancies are reflected in an RMSEP of 10.70 > RMSECV because the validation samples in RMSEP are completely new, while the RMSECV samples were used to build the model, which results in a more optimistic error estimation.

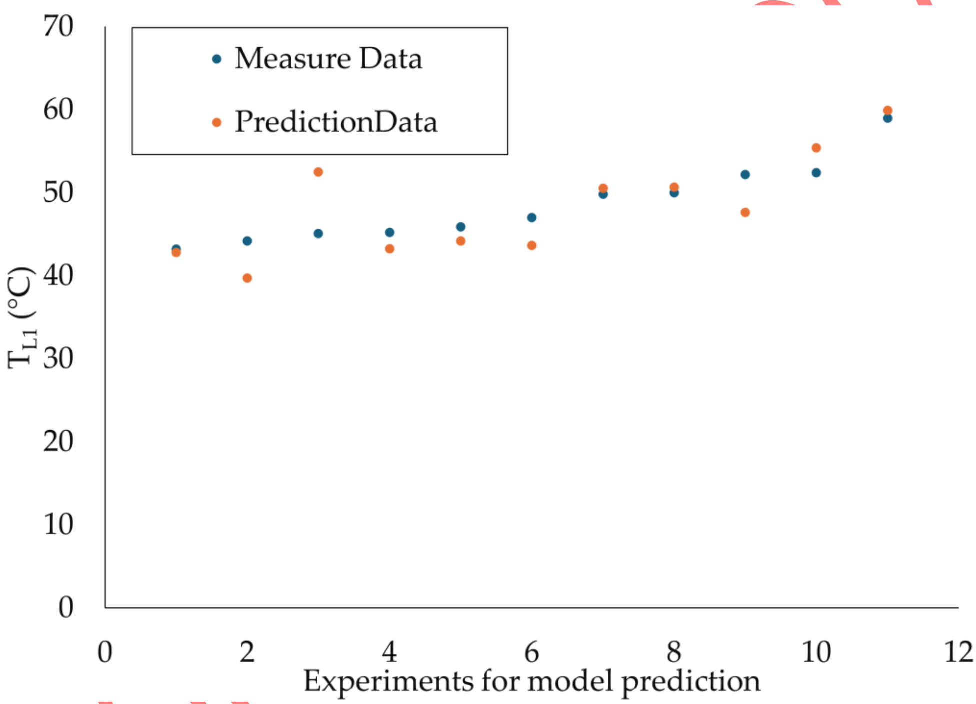

Figure 14. Comparison of predicted and measured Outlet Water Temperature.

The validation results, shown in Figure 15, indicate a good agreement between measured and calculated temperatures. Most of the validated data points are close to the measured values, with only minor deviations observed across the experimental range. The corresponding RMSECV for the validation dataset is 4.54, which can be considered low, indicating satisfactory predictive performance of the model under new operating conditions.

The difference in error magnitude between the prediction and validation datasets can be attributed to the sensitivity of the outlet water temperature estimation to multiple interacting parameters. The calculation of T_{L1} depends not only on the estimated volumetric mass transfer coefficient (k_ya), but also on uncontrolled parameters such as the flow patterns in each perforated fill and the change in humidity of the inlet air. Under certain operating conditions, small deviations in these parameters may result in notable differences in the predicted temperature, as observed in some prediction cases.

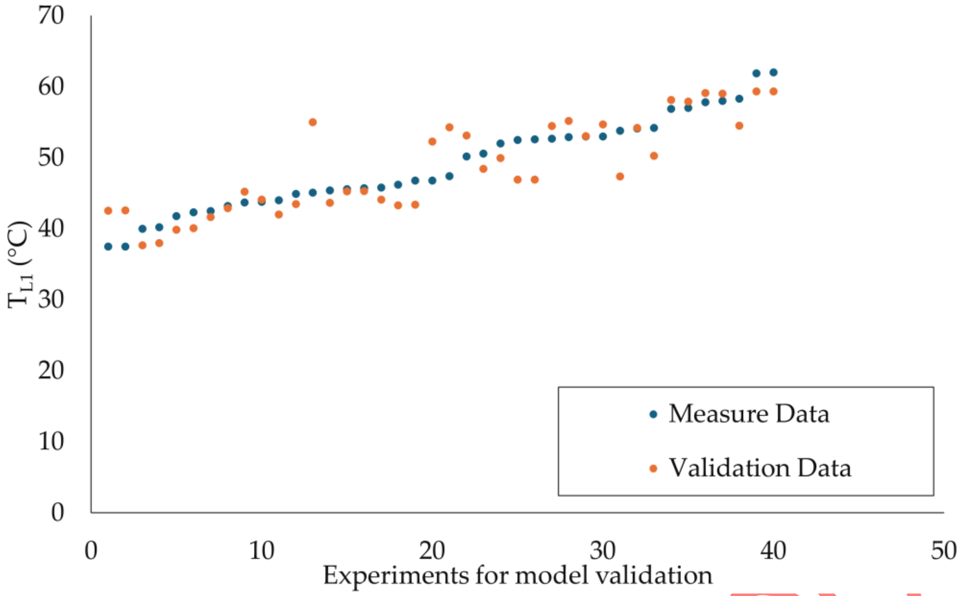

Figure 15. Comparison of validated and measured Outlet Water Temperature

Overall, the validation results demonstrate that, regardless of some deviations in the prediction dataset, the proposed model provides a reliable estimation of the outlet water temperature. This confirms the applicability of the developed k_ya correlation as a practical tool for predicting key thermal performance variables in cooling tower operation and pre-liminary design.

From a broader perspective, this methodology that combines laboratory experiments, detailed thermodynamic analysis, temperature profiling, and ANOVA, fits well with current trends that integrate high-quality experimental data with optimization for cooling water systems [22], [40]. Future work could extend the operating range, investigate alternative perforated plate geometries, and incorporate energy and exergy analyses to assess the overall sustainability of the tower in the context of process integration and decarbonization strategies [30], [41].

Finally, the experimental results confirm that the top water temperature T_{L2} is the main factor affecting the volumetric mass transfer coefficient in the studied cooling tower. This trend is coherent with the thermodynamic context explained in matherial and methods section, where the driving force for evaporation is expressed by the difference ($h_{yi} - h_y$) between the gas enthalpy in the interface with the bulk gas enthalpy.

The positive effect of liquid mass flow rate L on k_ya can be attributed to a better wetting of the perforated plates and to an increased effective contact area. Similar trends have been reported for film and splash fills, where higher liquid loadings improve wetting and reduce dry spots [3], [4]. However, the temperature profiles in Figures 8–10 show that, at high L, the lower stages of the column operate with high driving forces in terms of heat transfer while the upper stages are underutilized. In practical terms, this suggests that there is an optimum range of L that ensures adequate utilization of the tower height.

The limited influence of gas mass flow rate G on k_ya within the range 36–75 kg/h indicates that the system was operated with a sufficiently high air–to–water ratio. The current results support the recommendation to adjust G mainly based on energy efficiency, rather than mass transfer limitations, at least for laboratory-scale systems of similar sizes.

Limitation of the empirical correlation

The correlation proposed in this study to determine k_ya is empirical and was developed exclusively from the experimental data obtained for the cooling tower in this work. The applicability was limited to the operating ranges evaluated which are hot water inlet temperature T_{L2} = 50-70°C, air mass flow rate G = 36 – 75 kg/h, liquid mass flow rate L= 120

– 360 kg/h, and a fill geometry with acrylic inclined plates and multiple orifices. Extrapolation of the results outside these ranges is not recommended, since changes in the operating conditions or in the fill configuration might change the hydrodynamic behavior, water distribution, air-water contact, and heat and mass transfer mechanism inside the tower. Within the studied range, the liquid to gas mass flow ratio varied approximately from 1.6 to 10, covering a broad operating window for the evaluated system. Besides, the maximum air mass flow rate corresponded to an air velocity of approximately 0.79 – 0.86 m/s, which is well below the flooding point of the tower, estimated to be at 4 m/s. Thus, the experimental data, used to develop the correlation, were obtained under stable operating conditions, far from the flooding point.

The experimental operating conditions cover liquid to gas mass flow ratios from approximately 1.6 to 10, which represent a broad range of working conditions for the evaluated cooling tower. Also, the maximum air mass flow rate tested, G=75 kg/h, with the tower cross sectional area of 0.15x0.15 m^2, corresponds to an air mass flux of approximately 0.93 $kg/m^2 \cdot s$. Now, considering that the specific volume of the air for this system varies from 0.85 to 0.92 m3/kg of dry air, this corresponds to an air velocity ranging from approximately 0.79 and 0.86 m/s. These values are well below the flooding point of the tower, 4 m/s. Therefore, all the experiments were conducted under stable operating conditions, far from flooding.

CONCLUSIONS

A laboratory–scale mechanical–draft cooling tower equipped with perforated inclined plates was used to study the influence of operating conditions on the global volumetric mass transfer coefficient $k_y a$. A three–factor, three–level DOE was implemented, considering the liquid mass flow rate L, gas mass flow rate G, and top water temperature T_{L2}. From the experiments and the following statistical analysis, the next conclusions can be drawn:

- The volumetric mass transfer coefficient, $k_y a$, increased mainly with the hot water inlet temperature, T_{L2}, and to a lesser extent with the liquid mass flow rate, L. ANOVA confirmed that T_{L2} was the dominant factor followed by L within the evaluated operating conditions.
- In the assessed range of G from 36 to 75 kg/h, the gas mass flow rate showed a comparatively minor and statistically non-significant effect on $k_y a$. This finding is limited to the tested operating range and the specific fill geometry and should not be generalized to other cooling tower configurations.
- The best correlation for the studied tower is a power–law model based on the nominal gas flow rate, $\boldsymbol{k_y a = 6.59 \times 10^{-6} T_{L2}{}^{4.173} G^{0.149} L^{0.756}}$, which achieved R^2 = 0.869 and RMSEP = 5.93 × 10^3 kg/(m^3 h).
- The measured $k_y a$ values, ranging from approximately 4.6 × 10^3 to 6.2 × 10^4 kg/(m^3 h), are consistent with those reported in the literature for cooling towers, indicating that perforated inclined plates provide effective contact between water and air.
- For a liquid flow rate L = 120 kg/h, the gas and liquid temperature profiles exhibit almost linear behavior along the column height, with ΔT remaining relatively constant between sections. As the liquid inlet temperature T_{L2} increases and the flow rate L becomes larger, segments with steeper slopes are observed, especially for the air, indicating more intense evaporation in the lower region and dominant sensible cooling towards the upper part. Under conditions of low gas flow rate G and high T_{L2}, the T_G profile shows local curvature, reflecting a rapid approach to saturation.
- The developed model predicts with high reliability the outlet water temperature (T_{L1}), as shown by the low RMSEP=10.70 and RMSECV=4.54. Small prediction errors are mainly due to the sensitivity of T_{L1} to interacting operating parameters. Overall, the model is suitable for cooling tower performance analysis and preliminary design.

ACKNOWLEDGMENT(S)

The authors thank the staff of the Heat and Mass Transfer Laboratory at Universidad del Atlántico for their support during the experimental campaign.

NOMENCLATURE

Symbols

a	specific interfacial area per unit volume	[m²/m³]
A	fitted parameter in the numerical expression derived from the Merkel–Mickley method	—
B	fitted parameter in the numerical expression derived from the Merkel–Mickley method	—
F	F-ratio	—
G	gas mass flow rate	[kg/h]
G_s'	dry-air mass flux	[kg/(m²·h)]
h_L	liquid-side convective heat transfer coefficient	[kg/(m²·h)]
h_y	humid-air enthalpy in the bulk gas	[kJ/kg dry air]
h_{yi}	humid-air enthalpy at the gas–liquid interface	[kJ/kg dry air]
K	pre-exponential constant of the power-law correlation for ($k_y a$)	[depends on correlation]
$k_y a$	global volumetric mass transfer coefficient	[kg/(m³·h)]
L	liquid mass flow rate	[kg/h]
n	number of observations	—
p-value	observed probability ratio	—
Q	heat transfer rate	[kJ/h]
R^2	coefficient of determination	—
RMSE	root mean square error	[kg/(m³·h)]
RMSEP	root mean square error of prediction	[°C]
RMSECV	root mean square error of cross-validation	[°C]
T	temperature	[°C]
T_G	gas temperature	[°C]
T_i	interfacial temperature	[°C]
T_L	bulk liquid temperature	[°C]
T_{L1}	outlet water temperature	[°C]
T_{L2}	top/inlet water temperature	[°C]
Z	column height	[m]
dZ	differential column height	[m]

Greek letters

α-value	significance level	
α	exponent associated with (T_{L2}) in the power-law correlation	—
β	exponent associated with (G) in the power-law correlation	—
γ	exponent associated with (L) in the power-law correlation	—
Δ	differential	

Subscripts

exp	experimental
G	gas phase
i	interfacial condition
L	liquid phase
pred	predicted
s	superficial

y humid air basis
1 bottom column condition
2 top column condition

Abbreviations

ANOVA	Analysis of Variance
DF	Degrees of Freedom
DOE	Design of Experiments
MS	Mean Square
NTU	Number of Transfer Units
Pt100	Platinum resistance temperature detector
SS	Sum of Squares
VFD	Variable-Frequency Drive

REFERENCES

[1] S. Ghoddousi, A. Anderson, and B. Rezaie, "Advancing Water Conservation in Cooling Towers through Energy-Water Nexus," *European Journal of Sustainable Development Research*, vol. 5, no. 3, p. 161, 2021, doi: https://doi.org/10.21601/ejosdr/10952.

[2] J. U. R. Khan, M. Yaqub, and S. M. Zubair, "Performance characteristics of counter flow wet cooling towers," *Energy Convers. Manag.*, vol. 44, no. 13, pp. 2073–2091, Aug. 2003, doi: https://doi.org/10.1016/S0196-8904(02)00231-5.

[3] M. Lemouari, M. Boumaza, and A. Kaabi, "Experimental analysis of heat and mass transfer phenomena in a direct contact evaporative cooling tower," *Energy Convers. Manag.*, vol. 50, no. 6, pp. 1610–1617, Jun. 2009, doi: https://doi.org/10.1016/J.ENCONMAN.2009.02.002.

[4] Z. ; Hashemi *et al.*, "Recent Progress in Fill Media Technology for Wet Cooling Towers," *Processes 2023, Vol. 11, Page 2578*, vol. 11, no. 9, p. 2578, Aug. 2023, doi: https://doi.org/10.3390/PR11092578.

[5] H. A. Jenner, J. W. Whitehouse, C. J. L. Taylor, and M. Khalanski, "Cooling water management in European power stations Biology and control of fouling," *Hydroécologie Appliquée*, vol. 10, pp. I–225, 1998, doi: https://doi.org/10.1051/HYDRO:1989101.

[6] F. Merkel, "Evaporative cooling (German: Verdunstungskühlung)," Association of German Engineers, VDI (German), 70: 123-128, 1925.

[7] H. Jaber and R. L. Webb, "Design of Cooling Towers by the Effectiveness-NTU Method," *J. Heat Transfer*, vol. 111, no. 4, pp. 837–843, Nov. 1989, doi: https://doi.org/10.1115/1.3250794.

[8] J. C. Kloppers and D. G. Kröger, "Refinement of the Transfer Characteristic Correlation of Wet-Cooling Tower Fills," *Heat Transfer Engineering*, vol. 26, no. 4, pp. 35–41, May 2005, doi: https://doi.org/10.1080/01457630590916266.

[9] J. R. Picardo and J. E. Variyar, "The Merkel equation revisited: A novel method to compute the packed height of a cooling tower," *Energy Convers. Manag.*, vol. 57, pp. 167–172, May 2012, doi: https://doi.org/10.1016/J.ENCONMAN.2011.12.016.

[10] Y. She, G. Jiang, Z. Song, L. Zhao, and G. Liu, "Performance evaluation and optimization strategies of cooling water system considering ambient temperature," *Appl. Therm. Eng.*, vol. 279, p. 127785, Nov. 2025, doi: https://doi.org/10.1016/J.APPLTHERMALENG.2025.127785

[11] M. N. A. Hawlader and B. M. Liu, "Numerical study of the thermal–hydraulic performance of evaporative natural draft cooling towers," *Appl. Therm. Eng.*, vol. 22, no. 1, pp. 41–59, Jan. 2002, doi: https://doi.org/10.1016/S1359-4311(01)00065-5.

[12] E. Hajidavalloo, R. Shakeri, and M. A. Mehrabian, “Thermal performance of cross flow cooling towers in variable wet bulb temperature,” *Energy Convers. Manag.*, vol. 51, no. 6, pp. 1298–1303, Jun. 2010, doi: https://doi.org/10.1016/J.ENCONMAN.2010.01.005.

[13] M. A. Al-Nimr, “Dynamic thermal behaviour of cooling towers,” *Energy Convers. Manag.*, vol. 39, no. 7, pp. 631–636, May 1998, doi: https://doi.org/10.1016/S0196-8904(97)10006-1.

[14] W. F. He, L. N. Xu, D. Han, and L. Gao, “Performance analysis of an air-heated humidification–dehumidification desalination plant powered by low grade waste heat,” *Energy Convers. Manag.*, vol. 118, pp. 12–20, Jun. 2016, doi: https://doi.org/10.1016/J.ENCONMAN.2016.03.073.

[15] K. Singh and R. Das, “An experimental and multi-objective optimization study of a forced draft cooling tower with different fills,” *Energy Convers. Manag.*, vol. 111, pp. 417–430, Mar. 2016, doi: https://doi.org/10.1016/J.ENCONMAN.2015.12.080.

[16] F. Gharagheizi, R. Hayati, and S. Fatemi, “Experimental study on the performance of mechanical cooling tower with two types of film packing,” *Energy Convers. Manag.*, vol. 48, no. 1, pp. 277–280, Jan. 2007, doi: https://doi.org/10.1016/J.ENCONMAN.2006.04.002.

[17] H. R. Goshayshi and J. F. Missenden, “The investigation of cooling tower packing in various arrangements,” *Appl. Therm. Eng.*, vol. 20, no. 1, pp. 69–80, Jan. 2000, doi: https://doi.org/10.1016/S1359-4311(99)00011-3.

[18] R. F. F. Pontes, W. M. Yamauchi, and E. K. G. Silva, “Analysis of the effect of seasonal climate changes on cooling tower efficiency, and strategies for reducing cooling tower power consumption,” *Appl. Therm. Eng.*, vol. 161, p. 114148, Oct. 2019, doi: https://doi.org/10.1016/J.APPLTHERMALENG.2019.114148.

[19] N. Jourdan, M. Kanniche, T. Neveux, and O. Potier, “Experimental Characterization of Liquid Flows in Cooling Tower Packing,” *Ind. Eng. Chem. Res.*, vol. 61, no. 7, pp. 2926–2936, Feb. 2022, doi: https://doi.org/10.1021/ACS.IECR.1C04966.

[20] W. P. L. Cueva, D. B. S. Navarrete, K. A. T. Loor, G. V. A. Cabrera, W. O. E. Ramón, and E. J. G. Borja "Free software simulation of a forced-draft mechanical humidification tower to determine process parameters (Spanish: Simulación en software libre de una torre de humidificación de tiro mecánico forzado para determinar parámetros del proceso)," *Brazilian Journal of Development*, vol. 10, no. 10, Oct. 2024, doi: https://doi.org/10.34117/BJDV10N10-033.

[21] F. Táboas and F. Vázquez, “Pressure Drops and Energy Consumption Model of Low-Scale Closed Circuit Cooling Towers,” *Processes 2021, Vol. 9, Page 974*, vol. 9, no. 6, p. 974, May 2021, doi: https://doi.org/10.3390/PR9060974.

[22] F. Liu, T. Liu, and X. Feng, “Optimization of Circulating Cooling Water Network Revamping Considering Influence of Scaling,” *Chem. Eng. Trans.*, vol. 61, 2017, doi: https://doi.org/10.3303/CET1761220.

[23] K. V. Gololo and T. Majozi, “On Synthesis and Optimization of Cooling Water Systems with Multiple Cooling Towers,” *Ind. Eng. Chem. Res.*, vol. 50, no. 7, pp. 3775–3787, Apr. 2011, doi: https://doi.org/10.1021/IE101395V.

[24] J. Liang, L. Li, Y. Li, Y. Wang, and X. Feng, “Operation optimization of existing industrial circulating water system considering variable frequency drive,” *Chemical Engineering Research and Design*, vol. 186, pp. 387–397, Oct. 2022, doi: https://doi.org/10.1016/J.CHERD.2022.08.010.

[25] D. Niu, X. Liu, and Y. Tong, “Operation Optimization of Circulating Cooling Water System Based on Adaptive Differential Evolution Algorithm,” *International Journal of Computational Intelligence Systems 2023 16:1*, vol. 16, no. 1, pp. 22-, Feb. 2023, doi: https://doi.org/10.1007/S44196-023-00191-Z.

[26] Z. Lv, J. Cai, W. Sun, and L. Wang, “Analysis and Optimization of Open Circulating Cooling Water System,” *Water 2018, Vol. 10, Page 1592*, vol. 10, no. 11, p. 1592, Nov. 2018, doi: https://doi.org/10.3390/W10111592.

[27] L. Luo, P. Guo, and G. Wang, "3E (Energy–Exergy–Environmental) Performance Analysis and Optimization of Seawater Shower Cooling Tower for Central Air Conditioning Systems," *Processes 2025, Vol. 13, Page 1336*, vol. 13, no. 5, p. 1336, Apr. 2025, doi: https://doi.org/10.3390/PR13051336.

[28] Y. Liu, R. Shao, Q. Ye, J. Li, R. Sun, and Y. Zhai, "Optimization of an Industrial Circulating Water System Based on Process Simulation and Machine Learning," *Processes 2025, Vol. 13, Page 332*, vol. 13, no. 2, p. 332, Jan. 2025, doi: https://doi.org/10.3390/PR13020332.

[29] L. Yang *et al.*, "Thermal performance of counterflow wet cooling tower filled with inclined folding wave packing: An experimental and numerical investigation," *Int. J. Heat Mass Transf.*, vol. 235, p. 126151, Dec. 2024, doi: https://doi.org/10.1016/J.IJHEATMASSTRANSFER.2024.126151.

[30] M. Nakhaee Sharif, H. Goshayeshi, R. Saleh, I. Chaer, D. Toghraie, and S. Salahshoor, "Experimental study on the efficiency improvement of a forced draft wet cooling tower via magnetic Fe3O4 nanofluid and optimized packing," *Case Studies in Thermal Engineering*, vol. 74, p. 106904, Oct. 2025, doi: https://doi.org/10.1016/J.CSITE.2025.106904.

[31] P. DULCE PAULINA PADILLA MASCAREÑO Obregón, "Determination of the mass transfer coefficient in cooling towers (Spanish: Determinación del coeficiente de transferencia de masa en torres de enfriamiento)," Instituto tecnológico de Sonora, Obregón, 2013.

[32] L. G. Obregón Quiñones, J. C. Pertuz, R. A. Domínguez, L. G. Obregón Quiñones, J. C. Pertuz, and R. A. Domínguez, "Performance analysis of a laboratory-scale cooling tower for various packing materials, water inlet temperatures, and water-air mass flow ratios (Spanish: Análisis del desempeño de una torre de enfriamiento a escala de laboratorio para diversos materiales de empaque, temperatura de entrada de agua y relación másica de flujo agua-aire)," *Prospectiva*, vol. 15, no. 1, pp. 42–52, 2017, doi: https://doi.org/10.15665/RP.V15IL.820.

[33] Y. Cengel and A. Ghajar, *Heat and Mass Transfer: Fundamentals & Applications*, 5th ed. New York: McGraw Hill Education, 2015. Accessed: Jun. 06, 2026. [Online]. Available: https://www.scirp.org/reference/referencespapers?referenceid=1875128

[34] ASHRAE, *ASHRAE Handbook – HVAC Systems and Equipment*. Atlanta: American Society of Heating, Refrigerating and Air-Conditioning Engineers, 2020.

[35] D. C. Montgomery and J. Wiley, *Design and Analysis of Experiments Eighth Edition*, 8th ed. Hoboken: John Wiley & Sons, 2013. Accessed: Jun. 06, 2026. [Online]. Available: www.wiley.com/go/permissions.

[36] G. E. P. Box, J. S. Hunter, and W. G. Hunter, *Statistics for Experimenters: Design, Innovation, and Discovery*, 2nd ed. New Jersey: John Wiley & Sons, 2005.

[37] D. R. Baker and H. A. Shryock, "A Comprehensive Approach to the Analysis of Cooling Tower Performance," *J. Heat Transfer*, vol. 83, no. 3, pp. 339–349, Aug. 1961, doi: https://doi.org/10.1115/1.3682276.

[38] W. L. McCabe, J. C. Smith, and P. Harriott, *Unit Operations of Chemical Engineering*, 7th ed. New York: McGraw–Hill, 2007.

[39] R. E. Treybal, *Mass-Transfer Operations*, 3rd ed. New York: McGraw–Hill, 1980.

[40] J. J. Arenas Sarmiento, J. H. Herazo Acevedo, J. I. Silva Ortega, V. Sousa Santos, and J. E. Candelo-Becerra, "Energy Evaluation of Pumping Systems in a Clean Water Plant: A Case Study," *Journal of Sustainable Development of Energy, Water and Environment Systems*, vol. 11, no. 4, Dec. 2023, doi: https://doi.org/10.13044/J.SDEWES.D11.0466.

[41] B. Kilkis, "Exergy-optimum coupling of heat recovery ventilation units with heat pumps in sustainable buildings," *Journal of Sustainable Development of Energy, Water and Environment Systems*, vol. 8, no. 4, pp. 815–845, Dec. 2020, doi: https://doi.org/10.13044/J.SDEWES.D7.0316.